17. T. Wölfel *et al.*, *Science* **269**, 1281–1284 (1995).
18. S. H. van der Burg, M. J. Visseren, R. M. Brandt, W. M. Kast, C. J. Melief, *J. Immunol.* **156**, 3308–3314 (1996).
19. M. Harndahl *et al.*, *Eur. J. Immunol.* **42**, 1405–1416 (2012).
20. S. Kreiter *et al.*, *Nature* **520**, 692–696 (2015).
21. C. A. Klebanoff, S. A. Rosenberg, N. P. Restifo, *Nat. Med.* **22**, 26–36 (2016).

**ACKNOWLEDGMENTS**

We thank L. Fanchi, R. Mezzadra, and F. Scheeren for advice and support; A. Vefferstad and the OUH flow cytometry core facility for exemplary technical assistance; I. M. Svane for sharing clinical material; and the Norwegian Bone Marrow Donor Registry for HLA typing. The data presented in the manuscript are tabulated in the main paper and in the supplementary materials. DNA and RNA sequencing data have been deposited in the European Genome-Phenome Archive (accession codes EGAD00001000243 and EGAD00001000325). A patent application (P32649NL00) has been filed that covers the technology of targeting cancer-specific amino acid sequences with donor-derived TCR repertoires (inventors J.O., T.N.S., E.S., and M.T.). All described TCRs are available under an MTA with the Netherlands Cancer Institute and Oslo University Hospital. Supported by Dutch Cancer Society Queen Wilhelmina Award NKI 2013-6122 and EU H2020 project APERIM (T.N.S.); the K. G. Jebsen Foundation (J.O., T.N.S., F.L.-J.); and the Research Council of Norway, Regional Authorities South-Eastern Norway, the University of Oslo and Oslo University Hospital, and the Norwegian Cancer Society (J.O.).

**SUPPLEMENTARY MATERIALS**

www.sciencemag.org/content/352/6291/1337/suppl/DC1
Materials and Methods
Figs. S1 to S8
Tables S1 to S8
References (*22*–*43*)

17 January 2016; accepted 4 May 2016
Published online 19 May 2016
10.1126/science.aaf2288

DEVELOPMENT

# Zebrafish models of idiopathic scoliosis link cerebrospinal fluid flow defects to spine curvature

**D. T. Grimes,[1]* C. W. Boswell,[2,3]* N. F. C. Morante,[1]* R. M. Henkelman,[4,5] R. D. Burdine,[1] B. Ciruna[2,3]†**

**Idiopathic scoliosis (IS) affects 3% of children worldwide, yet the mechanisms underlying this spinal deformity remain unknown. Here we show that *ptk7* mutant zebrafish, a faithful developmental model of IS, exhibit defects in ependymal cell cilia development and cerebrospinal fluid (CSF) flow. Transgenic reintroduction of Ptk7 in motile ciliated lineages prevents scoliosis in *ptk7* mutants, and mutation of multiple independent cilia motility genes yields IS phenotypes. We define a finite developmental window for motile cilia in zebrafish spine morphogenesis. Notably, restoration of cilia motility after the onset of scoliosis blocks spinal curve progression. Together, our results indicate a critical role for cilia-driven CSF flow in spine development, implicate irregularities in CSF flow as an underlying biological cause of IS, and suggest that noninvasive therapeutic intervention may prevent severe scoliosis.**

Idiopathic scoliosis (IS) is a complex genetic disorder characterized by three-dimensional spinal curvatures, which arise in the absence of observable physiological or anatomical defects. Commonly diagnosed during adolescence, IS can cause disfigurement, reduced respiratory and pulmonary function, and chronic pain (*1*). In congenital and neuromuscular forms of scoliosis, spinal curves develop from vertebral malformations and/or underlying morbidities of the musculature and nervous system; however, the biological cause of IS has thus far remained unknown. As a result, treatment is limited to managing spinal deformity post-onset, through bracing and/or corrective surgery (*1*).

Genome-wide association studies have identified IS-associated polymorphisms in divergent human populations, but phenotypic and genetic variability have made it difficult to define causative mutations (*1*). Furthermore, a historical lack of appropriate animal models has confounded our basic understanding of the biology underlying IS (*2*). However, teleosts (bony fish) are, like humans, naturally prone to idiopathic spinal curvature (*3*), and recent genetic studies have identified faithful zebrafish IS models, providing important insights into the genetic causes of scoliosis (*4*, *5*) as well as a means to functionally validate human IS-associated genetic variants (*4*, *6*, *7*). Notably, zebrafish *ptk7* (protein tyrosine kinase-7) mutants present all defining attributes of the human disease, and studies of these mutants have implicated dysregulated Wnt signaling in the pathogenesis of IS (*4*).

Ptk7 is an essential regulator of both canonical Wnt–ß-catenin and noncanonical Wnt–planar cell polarity (PCP) signaling pathways (*8*). Although defects in either pathway are associated with a range of developmental abnormalities, both Wnt–PCP and Wnt–ß-catenin signaling have been implicated in the function of cilia (*9*–*11*). Cilia are microtubule-based organelles that project into the extracellular space and play critical roles in the perception and integration of environmental signals (*12*, *13*). Although most cell types elaborate short primary cilia, longer motile cilia are present on the surface of specialized cells and generate directional extracellular fluid flow in several contexts.

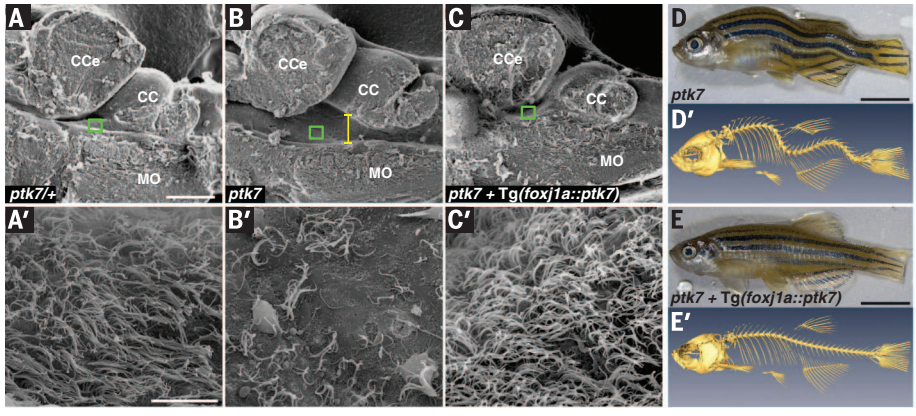


**Fig. 1. *ptk7* mutant fish exhibit hydrocephalus, EC cilia defects, and spinal curves, all of which are prevented by transgenic reintroduction of *ptk7* specifically in motile ciliated cell lineages.** (**A** to **C**) Representative sagittal SEM images of the brains of a *ptk7*/+ control [*n* = 6 (A)], a *ptk7* mutant [*n* = 6 (B)], and a *ptk7* mutant expressing Tg(*foxj1a*::*ptk7*) [*n* = 6 (C)], all at 2.5 months of age. The yellow line in (B) demarcates hydrocephalus. Green squares indicate the areas shown in corresponding high-magnification SEM images (**A′** to **C′**). (**D** to **E′**) Representative fixed [(D) and (E)] and μCT-rendered [(D′) and (E′)] lateral views of an adult *ptk7* mutant [(D) and (D′)] and an adult *ptk7* mutant expressing Tg(*foxj1a*::*ptk7*) [(E) and (E′)]. CCe, corpus cerebelli; CC, crista cerebellaris; MO, medulla oblongata. Scale bars, 250 μm [(A), (B), and (C)], 10 μm [(A′), (B′), and (C′)], and 5 mm [(D) and (E)].

[1]Department of Molecular Biology, Princeton University, Washington Road, Princeton, NJ 08544, USA. [2]Program in Developmental & Stem Cell Biology, The Hospital for Sick Children, 686 Bay Street, Toronto, Ontario M5G 0A4, Canada. [3]Department of Molecular Genetics, The University of Toronto, Toronto, Ontario M5S 1A8, Canada. [4]Mouse Imaging Centre, The Hospital for Sick Children, 25 Orde Street, Toronto, Ontario M5T 3H7, Canada. [5]Department of Medical Biophysics, The University of Toronto, Toronto, Ontario M5G 2M9, Canada.
*These authors contributed equally to this work. **†Corresponding author. Email: ciruna@sickkids.ca**

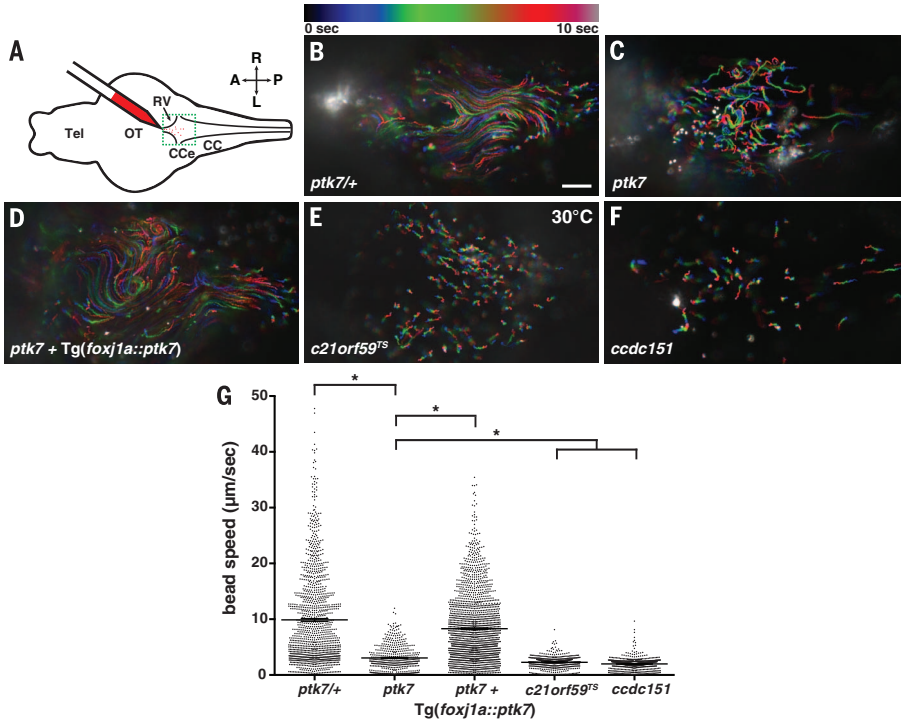


**Fig. 2. CSF flow is compromised in zebrafish IS models.** (**A**) Schematic of ventricular flow assay in whole-mount adult brains. The green dashed box represents the area imaged. (**B** and **C**) Bulk trajectory patterns of beads in whole-mount adult brains of *ptk7*/+ controls (B) and *ptk7* mutants (C). (**D**) Trajectory pattern of *ptk7* mutants expressing Tg(*foxj1a::ptk7*). (**E** and **F**) Trajectory patterns in additional IS models. In (B) to (F), trajectory paths are color-coded to represent initial position (blue) and final position (red) over 10 s. (**G**) Quantification of CSF flow in various IS models and controls, with data points representing an individual bead speed. Bars represent means. Standard errors of the means are as follows: *ptk7*/+, ±0.2352; *ptk7*, ±0.1013; *ptk7*+ Tg (*foxj1a::ptk7*), ± 0.1363; *c21orf59*$^{TS}$, ± 0.0374; and *ccdc15*, ±0.0342. Comparisons between genotypes used a *t* test. *$P < 0.0001$. A, anterior; L, left; OT, optic tectum; P, posterior; RV, rhombencephalic ventricle; R, right; Tel, telencephalon. Scale bar, 50 µm [(B) to (F)].

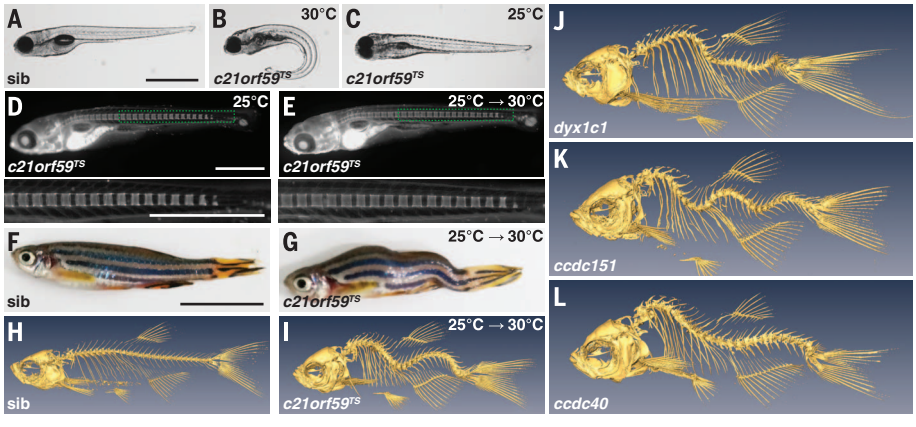


**Fig. 3. Cilia motility mutants exhibit spinal curves.** (**A** to **C**) Whereas sibling (sib) controls had no phenotype (A), mutant larvae from *c21orf59*$^{TS}$ intercrosses at 3 dpf exhibited cilia motility–associated defects, including ventral axis curvature, at 30°C (B) but not at 25°C (C). (**D** and **E**) Calcein staining of *c21orf59*$^{TS}$ mutants repaired during embryogenesis revealed no vertebral malformations during larval stages at either permissive [$n = 4$ (D)] or restrictive [$n = 7$ (E)] temperatures. Green rectangles indicate the areas shown in higher magnification below. (**F** and **G**) *c21orf59*$^{TS}$ mutants raised at 25°C until 5 dpf and then shifted to 30°C exhibited spinal curves at sexual maturity [$n = 10$ (G)] that were not present in sib controls [$n = 3$ (F)]. (**H** and **I**) µCT of sib controls [$n = 3$ (H)] and *c21orf59*$^{TS}$ mutants raised at 25°C until 5 dpf and then shifted to 30°C [$n = 10$ (I)]. (**J** to **L**) µCT of *dyx1c1* mutants [($n = 3$ (J)], *ccdc151* mutants [$n = 7$ (K)], and *ccdc40* mutants [$n = 3$ (L)], repaired during embryonic stages by injection of wild-type mRNA at the one-cell stage. Scale bars, 1 mm [(A) to (E)] and 1 cm [(F) and (G)].

Cilia-directed flow within early embryonic organizers breaks left-right (L-R) symmetry in development (*14*), and cerebrospinal fluid (CSF) flow, which is critical for central nervous system homeostasis (*15*), is generated by the polarized beating of ependymal cell (EC) cilia lining brain ventricles (*16*). Abnormal L-R asymmetries and defective CSF flow have been observed in IS patients (*17*), and an elevated incidence of scoliosis has been documented among primary ciliary dyskinesia patients (*18*). We therefore hypothesized that motile cilia dysfunction may contribute to the etiopathogenesis of IS.

To test this, we first investigated EC motile cilia structure and function in scoliotic *ptk7* mutant zebrafish and sibling *ptk7*/+ controls. Examination of *ptk7* mutant brain ventricles by scanning electron microscopy (SEM) revealed severe hydrocephalus (Fig. 1, A and B), a phenotype commonly associated with loss of EC cilia function (*16*). Moreover, whereas a dense network of polarized EC cilia lined the ventral surface of *ptk7*/+ ventricles, cilia in *ptk7* mutant ventricles were sparse and, when present, lacked posterior polarization (Fig. 1, A′ and B′). To directly examine the consequence of EC cilia defects, we tracked fluorescent microsphere movement across the ventral surface of the rhombencephalic ventricle (Fig. 2A). Dynamic anterior-to-posterior flow was observed across the ventricle of *ptk7*/+ brains (Fig. 2, B and G, and movie S1). In contrast, although some movement was observed during particle tracking in *ptk7* mutants, microspheres exhibited irregular trajectories and significantly reduced speeds (Fig. 2, C and G, and movie S2). These results demonstrate abnormal CSF flow within the ventricular system of scoliotic *ptk7* mutants and are consistent with a role for EC motile cilia defects in the etiology of IS.

To investigate whether scoliosis specifically results from motile cilia dysfunction, we assessed potential amelioration of *ptk7* mutant spinal curves through transgenic reintroduction of wild-type Ptk7 in motile ciliated cell lineages only. The transcription factor FoxJ1a is a master regulator of motile ciliogenesis (*19*). We therefore cloned and characterized a *foxj1a* enhancer element that specifically drives transgene (Tg) expression in all known sites of motile cilia formation, as demonstrated in multiple *foxj1a::eGFP* transgenic lines (eGFP, enhanced green fluorescent protein) (fig. S1, A to D, and movie S3). Along the trunk of juvenile animals, Tg(*foxj1a::eGFP*) expression was predominantly restricted to midline structures of the brain and spinal cord. We next generated four independent *foxj1a::ptk7* stable transgenic lines (fig. S1E) and found that the presence of Tg(*foxj1a::ptk7*) restored EC cilia and CSF flow in *ptk7* mutant fish and prevented hydrocephalus from manifesting (Fig. 1, C and C′; Fig. 2, D and G; and movie S4). Importantly, spinal curve formation, assessed by micro-computed tomography (µCT), was also fully suppressed by the transgenes ($n = 59$; Fig. 1, D to E′), showing that scoliosis in mutants is specifically caused by Ptk7 dysfunction in motile ciliated lineages.

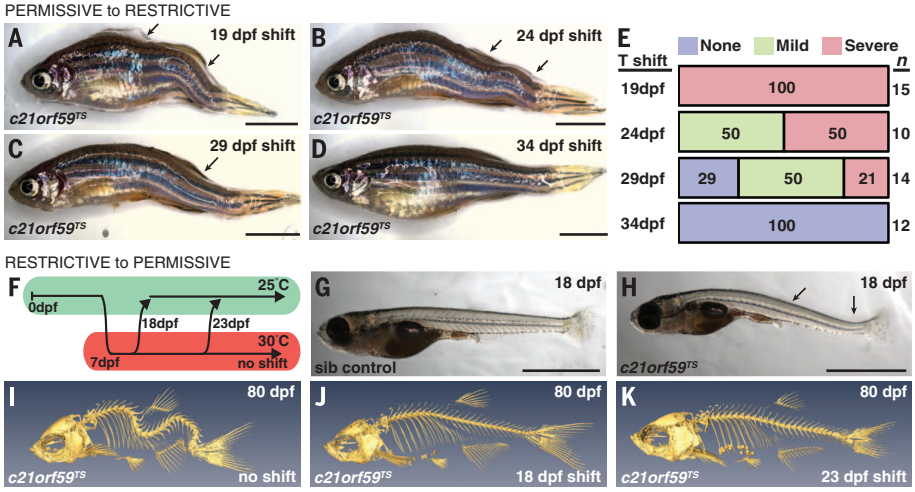


**Fig. 4. Temporal window for motile cilia function in spine development.** (**A** to **D**) Representative lateral views of *c21orf59*$^{TS}$ mutants that were shifted from 25°C to 30°C at 19 dpf (A), 24 dpf (B), 29 dpf (C), and 34 dpf (D). (**E**) Quantification of scoliosis phenotypes in temperature-shifted mutants, observed at 6 months post-fertilization (numbers are percentages). (**F**) Schematic of restrictive (30°C)–to–permissive (25°C) temperature shift experiments performed with *c21orf59*$^{TS}$ mutants. (**G** and **H**) Lateral images of a juvenile sib control (G) and a *c21orf59*$^{TS}$ mutant (H), both kept at 30°C, show curve initiation in mutants by 18 dpf. (**I**) Representative μCT image of an 80-dpf unshifted *c21orf59*$^{TS}$ mutant. (**J** and **K**) Representative μCT images of 80-dpf *c21orf59*$^{TS}$ mutants shifted from 30°C to 25°C at 18 dpf [*n* = 6 (J)] or at 23 dpf [*n* = 6 (K)]. Scale bars, 5 mm [(A) to (D)] and 2 mm [(G) and (H)].

If cilia motility defects contribute to IS pathogenesis, then *ccdc40* (*20*), *ccdc151* (*21*), *dyx1c1* (*22*), and *c21orf59* (*23*, *24*) mutations, which all disrupt cilia motility, should lead to the development of scoliosis. However, aberrant cilia motility causes a characteristic suite of embryonic phenotypes that usually result in death by 1 to 2 weeks of development (*20*, *21*), precluding analysis of adolescent spine formation. To circumvent this early lethality, we used two strategies. First, we took advantage of the *c21orf59* temperature-sensitive mutation *tm304*, here called *c21orf59*$^{TS}$ (*24*). At 30°C (a restrictive temperature), *c21orf59*$^{TS}$ mutant embryos exhibited abnormal cilia motility and associated developmental defects (Fig. 3, A and B). However, at 25°C (a permissive temperature), *c21orf59*$^{TS}$ embryos retained cilia motility and could develop normally (Fig. 3C) (*24*). *c21orf59*$^{TS}$ mutants that were raised at 25°C for 5 days to prevent embryonic defects and then shifted to 30°C resembled wild-type zebrafish through the larval stages, exhibiting normal vertebral formation, as monitored using the vital fluorescent $Ca^{2+}$-binding chromophore calcein (Fig. 3, D and E). CSF flow in the rhombencephalic ventricle of these *c21orf59*$^{TS}$ mutants was severely compromised (Fig. 2, E and G, and movie S5). Moreover, all mutant fish developed spinal curves that began to form during early juvenile stages (3 to 4 weeks of age; fig. S2, A and B) and that model defining attributes of IS (Fig. 3, F to I, and movie S6).

Our second strategy involved suppressing embryonic phenotypes by means of RNA injections at the one-cell stage and analyzing mutants during adolescence. Using CRISPR/Cas9 gene targeting, we generated a *dyx1c1* mutant allele (fig. S3). Functional characterization of *dyx1c1* mutants revealed abnormal cilia motility and associated developmental defects, including embryonic lethality (fig. S3, C to F), in agreement with gene knockdown studies (*22*). *dyx1c1* mutants injected with wild-type mRNA to prevent embryonic defects developed severe three-dimensional spinal curvatures in the absence of congenital vertebral malformations (Fig. 3J; fig. S2, A and B; and fig. S4). Furthermore, *ccdc151* and *ccdc40* mutant embryos that were phenotypically normal in embryonic stages (owing to wild-type mRNA injection) also developed late-onset spinal curves that model IS (Fig. 3, K to L). Our demonstration that mutations in four different genes, each of which has been shown to disrupt cilia motility, all yield similar adolescent spinal curve phenotypes provides strong evidence that motile cilia dysfunction represents the underlying cell-biological cause of IS in these models.

These experiments further demonstrate a post-embryonic requirement for motile cilia in spine morphogenesis. Transient knockdown of Dyx1c1 or Ccdc151 through only the first 3 to 4 days of embryogenesis [by injection of translation-blocking antisense morpholino oligonucleotides (MOs)] did not result in adolescent spinal curvatures, despite the fact that MO-injected embryos phenocopied genetic mutants during early embryogenesis (fig. S5). To define the critical developmental window for motile cilia function in the etiopathogenesis of IS, we performed a series of temperature shift experiments using the *c21orf59*$^{TS}$ mutant allele. *c21orf59*$^{TS}$ mutant embryos were raised at 25°C for at least 5 days (to prevent embryonic phenotypes), transferred to a restrictive temperature (30°C) at defined incremental stages of development, and screened for spinal curvatures at sexual maturity (Fig. 4, A to D). *c21orf59*$^{TS}$ mutants that were shifted to restrictive temperatures at 19 days post-fertilization (dpf) all developed severe spinal curves by 5 weeks of age (Fig. 4, A and E). In contrast, *c21orf59*$^{TS}$ mutants that were shifted to 30°C at 24 and 29 dpf exhibited milder spinal curvatures (Fig. 4, B, C, and E), whereas *c21orf59*$^{TS}$ mutants that were shifted to 30°C at 34 dpf displayed no signs of scoliosis through the adult stages (Fig. 4, D and E). These results indicate a finite and temporally defined requirement for motile cilia function during spine morphogenesis. This time interval correlates with documented periods of accelerated adolescent growth (*4*), when spinal curves typically manifest in IS.

Last, to determine whether restoration of motile cilia function can prevent severe spinal curve progression after the onset of scoliosis, we performed restrictive-to-permissive temperature shifts at defined time points. *c21orf59*$^{TS}$ mutant embryos were first raised at 25°C until 7 dpf to allow normal embryonic development, transferred to 30°C until the onset of spinal curve formation, and then returned to permissive temperatures at incremental stages of spinal curve progression (Fig. 4, F to H). Restoration of motile cilia activity at the onset of scoliosis blocked spinal curve progression (Fig. 4, J to K). This provides a proof-of-principle that the development of severe IS spinal curvatures can be managed without invasive surgical manipulation.

The data presented here demonstrate that cilia motility is required for zebrafish spine morphogenesis. Given the acute hydrocephalus and EC cilia defects observed in *ptk7* mutants, the predominant expression of *foxj1a* transgenes throughout the brain and spinal cord of juvenile animals, and the severe CSF flow defects observed across zebrafish IS models, we suggest that irregularities in CSF flow represent the underlying cell-biological cause of IS. Several observations support this model: (i) Disruption of CSF activity via Kaolin injection into the subarachnoid space can cause scoliosis in both dog and rabbit models (*25*, *26*), and (ii) scoliosis is highly prevalent in multiple human conditions associated with obstructed CSF flow, including Chiari malformation, syringomyelia, and myelomeningoceles (*27*–*29*). Our data explain these observations and further imply an evolutionarily conserved role for CSF flow in spine morphogenesis, thus warranting reexamination of the anatomy, physiology, and genetics of CSF flow in cases of human IS. Downstream of CSF flow, molecular mechanisms influencing spine morphogenesis remain to be determined but could involve multiple gene products that have been previously associated with IS [e.g., potential motile cilia functions for the centriolar protein POC5 (*6*) or chondrocyte-specific activation of GPR126 (*30*)]. Ultimately, our demonstration that severe spinal curvatures can be prevented with the restoration of motile cilia activity may have important therapeutic ramifications; pharmaceutical manipulation of the production and/or downstream interpretation of CSF signals could potentially stop severe

spinal curve progression in some IS patients, even after the onset and clinical diagnosis of scoliosis.

## REFERENCES AND NOTES


1. J. C. Cheng *et al.*, *Nat. Rev. Dis. Prim.* **1**, 15030 (2015).
2. M. M. Janssen, R. F. de Wilde, J. W. Kouwenhoven, R. M. Castelein, *Spine J.* **11**, 347–358 (2011).
3. K. F. Gorman, F. Breden, *Med. Hypotheses* **72**, 348–352 (2009).
4. M. Hayes *et al.*, *Nat. Commun.* **5**, 4777 (2014).
5. J. G. Buchan *et al.*, *Dev. Dyn.* **243**, 1646–1657 (2014).
6. S. A. Patten *et al.*, *J. Clin. Invest.* **125**, 1124–1128 (2015).
7. S. Sharma *et al.*, *Nat. Commun.* **6**, 6452 (2015).
8. M. Hayes, M. Naito, A. Daulat, S. Angers, B. Ciruna, *Development* **140**, 1807–1818 (2013).
9. T. J. Park, B. J. Mitchell, P. B. Abitua, C. Kintner, J. B. Wallingford, *Nat. Genet.* **40**, 871–879 (2008).
10. A. Borovina, S. Superina, D. Voskas, B. Ciruna, *Nat. Cell Biol.* **12**, 407–412 (2010).
11. A. Caron, X. Xu, X. Lin, *Development* **139**, 514–524 (2012).
12. V. Singla, J. F. Reiter, *Science* **313**, 629–633 (2006).
13. S. C. Goetz, K. V. Anderson, *Nat. Rev. Genet.* **11**, 331–344 (2010).
14. J. J. Essner *et al.*, *Nature* **418**, 37–38 (2002).
15. M. J. Simon, J. J. Iliff, *Biochim. Biophys. Acta* **1862**, 442–451 (2016).
16. L. Lee, *J. Neurosci. Res.* **91**, 1117–1132 (2013).
17. W. J. Wang *et al.*, *J. Pediatr. Orthop.* **31**, S14–S27 (2011).
18. V. G. Engesaeth, J. O. Warner, A. Bush, *Pediatr. Pulmonol.* **16**, 9–12 (1993).
19. S. P. Choksi, G. Lauter, P. Swoboda, S. Roy, *Development* **141**, 1427–1441 (2014).
20. A. Becker-Heck *et al.*, *Nat. Genet.* **43**, 79–84 (2011).
21. R. Hjeij *et al.*, *Am. J. Hum. Genet.* **95**, 257–274 (2014).
22. A. Tarkar *et al.*, *Nat. Genet.* **45**, 995–1003 (2013).
23. C. Austin-Tse *et al.*, *Am. J. Hum. Genet.* **93**, 672–686 (2013).
24. K. M. Jaffe *et al.*, *Cell Rep.* **14**, 1841–1849 (2016).
25. A. Chuma *et al.*, *Spine* **22**, 589–594, discussion 595 (1997).
26. M. Turgut, E. Cullu, A. Uysal, M. E. Yurtseven, B. Alparslan, *Neurosurg. Rev.* **28**, 289–297 (2005).
27. T. H. Milhorat *et al.*, *Neurosurgery* **44**, 1005–1017 (1999).
28. R. A. Ozerdemoglu, F. Denis, E. E. Transfeldt, *Spine* **28**, 1410–1417 (2003).
29. M. Verhoef *et al.*, *Dev. Med. Child Neurol.* **46**, 420–427 (2004).
30. C. M. Karner, F. Long, L. Solnica-Krezel, K. R. Monk, R. S. Gray, *Hum. Mol. Genet.* **24**, 4365–4373 (2015).


## ACKNOWLEDGMENTS


We gratefully acknowledge E. Lee, D. Holmyard, P. Paroutis, and L. Yu for technical assistance; A. Morley, A. Ng, C. Hasty, D. Bosco, and P. Johnson for zebrafish care; and J. Schottenfeld-Roames and T. Ku for initial observations of spine curvatures in *c21orf59*$^{TS}$ mutant fish. This work was supported in part by funding from the Canada Research Chairs program to R.M.H. and B.C.; National Institute of Child Health and Development grant 2R01HD048584 to R.D.B.; and Canadian Institutes of Health Research (MOP-111075) and March of Dimes Foundation (#1-FY13-398) grants to B.C. D.T.G., C.W.B., and N.F.C.M. performed all experiments characterizing scoliosis phenotypes. C.W.B. cloned and characterized *foxj1a* transgenic lines. N.F.C.M. generated the *dyx1c1*$^{pr13}$ allele. C.W.B. and R.M.H. performed μCT. B.C. and C.W.B. performed SEM and CSF flow analyses. D.T.G., C.W.B., N.F.C.M., R.D.B., and B.C. analyzed the data. D.T.G., C.W.B. and B.C. wrote the manuscript, and all authors edited the manuscript.


## SUPPLEMENTARY MATERIALS

www.sciencemag.org/content/352/6291/1341/suppl/DC1
Materials and Methods
Figs. S1 to S5
Movies S1 to S6
References (*31*–*33*)


8 March 2016; accepted 16 May 2016
10.1126/science.aaf6419


CANCER

# The histone H3.3K36M mutation reprograms the epigenome of chondroblastomas


**Dong Fang,[1]* Haiyun Gan,[1]* Jeong-Heon Lee,[1,2]* Jing Han,[1]* Zhiquan Wang,[1]* Scott M. Riester,[3] Long Jin,[3] Jianji Chen,[4] Hui Zhou,[1] Jinglong Wang,[5,6] Honglian Zhang,[1] Na Yang,[5] Elizabeth W. Bradley,[3] Thai H. Ho,[7] Brian P. Rubin,[8] Julia A. Bridge,[9] Stephen N. Thibodeau,[10] Tamas Ordog,[2,11,12] Yue Chen,[4] Andre J. van Wijnen,[1,3] Andre M. Oliveira,[3,10] Rui-Ming Xu,[5,6] Jennifer J. Westendorf,[1,3] Zhiguo Zhang[1,2]†**



**More than 90% of chondroblastomas contain a heterozygous mutation replacing lysine-36 with methionine-36 (K36M) in the histone H3 variant H3.3. Here we show that H3K36 methylation is reduced globally in human chondroblastomas and in chondrocytes harboring the same genetic mutation, due to inhibition of at least two H3K36 methyltransferases, MMSET and SETD2, by the H3.3K36M mutant proteins. Genes with altered expression as well as H3K36 di- and trimethylation in H3.3K36M cells are enriched in cancer pathways. In addition, H3.3K36M chondrocytes exhibit several hallmarks of cancer cells, including increased ability to form colonies, resistance to apoptosis, and defects in differentiation. Thus, H3.3K36M proteins reprogram the H3K36 methylation landscape and contribute to tumorigenesis, in part through altering the expression of cancer-associated genes.**


Chondroblastomas are locally recurrent primary bone tumors (*1*). Recently, it has been reported that one allele of the *H3F3B* gene, one of two genes encoding histone H3 variant H3.3 (*2*, *3*), is frequently mutated in chondroblastoma (*4*). In addition, global reductions of di- and trimethylation of histone H3 at lysine-36 (H3K36me2 and H3K36me3) of endogenous histone H3 in mammalian cells exogenously expressing the H3.3 Lys$^{36}$→Met$^{36}$ (H3.3K36M) mutant protein have been observed (*5*, *6*). However, the mechanism by which the mutant proteins exert their effects on H3K36 methylation of endogenous histones and how the H3.3K36M mutation promotes tumorigenesis of this poorly studied tumor are largely unknown.

We used H3K36me2- and H3K36me3-specific antibodies (fig. S1) to analyze the levels of H3K36me2 and H3K36me3 in three primary human chondroblastomas harboring the H3.3K36M mutation and in three giant cell tumors with the H3.3G34W (Gly$^{34}$→Trp$^{34}$) mutation (table S1). H3K36me2 and H3K36me3 were globally reduced in each chondroblastoma specimen, but not in giant cell tumors or normal bone tissues (Fig. 1A).

We used the CRISPR/Cas9 system (*7*) to introduce the H3.3K36M mutation into one *H3F3B* allele (fig. S2) of T/C28a2 cells, which are immortalized human chondrocytes (*8*). The levels of H3K36me1, H3K36me2, and H3K36me3 were reduced in two independent mutant cell lines, as compared with methylation levels in parental T/C28a2 cells (Fig. 1B and fig. S3). As determined by mass spectrometric analysis, H3K36me2 was reduced more substantially than H3K36me3 (fig. S3, A and B). No apparent changes were observed in H3K4me3, H3K9me3, H3K27me3, or H4K20me3 (Fig. 1B). These results demonstrate that the global reduction of H3K36 methylation in tumor tissues results from the expression of H3.3K36M mutant proteins.

To understand how H3.3K36M mutant proteins globally reduce H3K36 methylation, we first tested the ability of a H3.3K36M peptide to inhibit the enzymatic activities of four human H3K36 methyltransferases—SETD2, ASH1L, MMSET/WHSC1, and NSD1—which catalyze H3K36me1, H3K36me2, and H3K36me3 (*9*–*11*). The purified catalytic domains of each enzyme exhibited methyltransferase activities against H3.3-containing mononucleosomes. The H3.3K36M peptide inhibited the


[1]Department of Biochemistry and Molecular Biology, Mayo Clinic College of Medicine, 200 First Street SW, Rochester, MN 55905, USA. [2]Epigenomics Program, Center of Individualized Medicine, Mayo Clinic College of Medicine, 200 First Street SW, Rochester, MN 55905, USA. [3]Department of Orthopedic Surgery, Mayo Clinic College of Medicine, 200 First Street SW, Rochester, MN 55905, USA. [4]Department of Biochemistry, Molecular Biology, and Biophysics, University of Minnesota at Twin Cities, Minneapolis, MN 55455, USA. [5]National Laboratory of Biomacromolecules, Institute of Biophysics, Chinese Academy of Sciences, 5 Datun Road, Beijing 100101, China. [6]University of Chinese Academy of Sciences, 19A Yuquan Road, Beijing 100049, China. [7]Division of Hematology/Oncology, Mayo Clinic Arizona, 13400 East Shea B., Scottsdale, AZ 85259, USA. [8]Robert J. Tomsich Pathology and Laboratory Medicine Institute and Department of Cancer Biology, Cleveland Clinic and Lerner Research Institute, L2 9500 Euclid Avenue, Cleveland, OH 44195, USA. [9]Departments of Pathology and Microbiology, Pediatrics, and Orthopaedic Surgery and Rehabilitation. [10]Department of Laboratory Medicine and Pathology, Mayo Clinic College of Medicine, 200 First Street SW, Rochester, MN 55905, USA. [11]Department of Physiology and Biomedical Engineering, Division of Gastroenterology and Hepatology, Mayo Clinic College of Medicine, 200 First Street SW, Rochester, MN 55905, USA. [12]Interdisciplinary Health Science Initiative, 1110 Micro and Nanotechnology Laboratory, M/C 249, University of Illinois Urbana-Champaign, Urbana, IL 61801, USA.
*These authors contributed equally to this work. **†Corresponding author. Email: zhang.zhiguo@mayo.edu**

Science

# Zebrafish models of idiopathic scoliosis link cerebrospinal fluid flow defects to spine curvature

D. T. Grimes, C. W. Boswell, N. F. C. Morante, R. M. Henkelman, R. D. Burdine and B. Ciruna

*Science* **352** (6291), 1341-1344.
DOI: 10.1126/science.aaf6419

**Altered fluid flow causes curved spine**

Adolescent idiopathic scoliosis is characterized by three-dimensional spinal curves and affects 3% of the world's children. However, the biological basis of this condition is unclear. Grimes *et al.* studied zebrafish models that likewise display a curved spine. Defects in the formation and function of motile cilia in the central nervous system perturbed the flow of cerebrospinal fluid (CSF), leading to abnormal spinal curvatures as the fish grew. Curves could be partially rescued by restoring CSF flow, suggesting potential therapeutic strategies if the same mechanism is shared in humans.

*Science*, this issue p. 1341